Ali, Abdelfatah; Mahmoud, Karar; Lehtonen, Matti

Multi-objective Photovoltaic Sizing with Diverse Inverter Control Schemes in Distribution Systems Hosting EVs

Published in:
IEEE Transactions on Industrial Informatics

DOI:
10.1109/TII.2020.3039246

Published: 01/09/2021

Document Version
Peer reviewed version

Please cite the original version:
Ali, A., Mahmoud, K., & Lehtonen, M. (2021). Multi-objective Photovoltaic Sizing with Diverse Inverter Control Schemes in Distribution Systems Hosting EVs. *IEEE Transactions on Industrial Informatics*, *17*(9), 5982-5992. [9264759]. https://doi.org/10.1109/TII.2020.3039246

Multi-objective Photovoltaic Sizing with Diverse Inverter Control Schemes in Distribution Systems Hosting EVs

Abdelfatah Ali, Karar Mahmoud, and Matti Lehtonen

***Abstract*— Worldwide, photovoltaic (PV) and electric vehicles (EVs) have intensively been integrated into distribution systems. As a result, different operational issues can be observed due to PV generation variability and EV stochastic characteristics. In this work, an optimal sizing approach of multiple PVs in the existence of EVs is proposed. The proposed approach minimizes both the total voltage deviations and overall energy losses, prevents active PV power curtailment, and considers numerous constraints of PV, EV, and the distribution system. The features of the proposed approach are the considerations of PV, EV, and load uncertainties via incorporating their probabilistic models. Besides, it models arrival/parting times of EVs, the required state of charge (SOC) of EV batteries based on initial SOCs and remaining parking periods, and controlled/uncontrolled charging. Furthermore, diverse control schemes of the interfacing PV inverter are formulated in the proposed optimization model. To effectively solve this comprehensive model with conflicting sub-functions and variables, a two-level multi-objective evolutionary algorithm based on decomposition with fuzzy sets is developed. The upper optimization level accurately optimizes the sizes of multiple PVs while the lower one optimizes charging/discharging of EV batteries, PV inverter oversize, and PV reactive power. The results prove the effectiveness of the proposed approach.**

***Index Terms*— Distribution systems, electric vehicle, photovoltaic, voltage deviations, energy losses.**

Nomenclature

Abbreviations

CPVL	combined PV-load probability
DOD	depth of discharge
EVs	electric vehicles
MOP	multi-objective optimization problem
MOEA/D	multi-objective evolutionary algorithm based on decomposition
PV	Photovoltaic
RES	renewable energy sources
SOC	state of charge
VD	voltage deviation
MPPT	maximum power point tracking

Variables

f_1	sub-objective of total energy losses
f_2	sub-objective of voltage deviation
s	represents the states of the CPVL
$E^t_{l,s}$	energy losses of state *s*
$P^t_{l.s}$	active power losses of state *s*
$\Delta\tau$	time durations (one hour)
$P^t_{comb}(\lambda_s)$	CPVL for state *s* of time duration *t*
λ	a double-column matrix including the whole groupings of the PV and load states
n_t	number of time durations
n_s	number of all states
$P_{Curt,i}$	active PV power curtailment of unit *i*
$P^{max}_{Curt,i}$	maximum curtailment rate of unit *i*
$S_{inv,i}$	interfacing PV inverter rating of unit *i*
$S^{min}_{Inv,i}, S^{max}_{Inv,i}$	allowed boundaries of the inverter size
$C_{PV,i}$	size of PV unit *i*
$Q_{PV,i}$	reactive power of interfacing inverter *i*
R^{max}_{PV}	maximum total PV size
$P^{min,t}_{Station,i}$	lower limit EVs active power exchange
$P^{max,t}_{Station,i}$	upper limit EVs active power exchange
$P^t_{Station,i,s}$	active power exchange of EVs
$SOC^t_{n,s}$	current SOC of n^{th} EV battery
SOC^{Dep}_n	SOC value of n^{th} battery at the parting time
SOC^{min}_n	minimum required SOC at parting time
$P^t_{ij,s}$	active power flows through branch *ij*
$Q^t_{ij,s}$	reactive power flows through branch *ij*
$P^t_{PV,i,s}$	active power of PV
$P^t_{d,s}$	active power of load
$Q^t_{Load,i}$	reactive power of load
n_b	numbers of buses
N_{PV}	numbers of PV units
V_n	nominal voltage
V^{min}, V^{max}	lower and upper voltage boundaries
$V^t_{0,s}$	voltage of main substation
$\delta^t_{0,s}$	angle of main substation
$P^t_{o,s}$	active power of main substation
$Q^t_{o,s}$	reactive power of main substation
$I^t_{ij,s}$	current flows through line *ij*
$P^t_{ch,n,s}$	charging power rate of n^{th} battery
$P^t_{dc,n,s}$	discharging power rate of n^{th} battery
$\eta_{ch,n}$	efficiency of charging mode
$\eta_{dc,n}$	efficiency of discharging mode
$C_{batt,n}$	rated capacity of battery *n*
$T_{arr,n}$	arrival instant
$T_{d,n}$	parting instant
μ^t_{Tarr}, σ^t_{Tarr}	mean and standard deviation of daily arrival instant
dm_n	daily mileage
AER_n	all-electric range

A. Ali is with the Faculty of Engineering, South Valley University, 83523 Qena, Egypt (e-mail: a.ahmed@eng.svu.edu.eg).

K. Mahmoud is with the Department of Electrical Engineering and Automation, Aalto University, FI-00076 Espoo, Finland, and also with the Faculty of Engineering, Aswan University, 81542 Aswan, Egypt (e-mail: karar.mostafa@aalto.fi).

M. Lehtonen is with the Department of Electrical Engineering and Automation, Aalto University, FI-00076 Espoo, Finland (email: matti.lehtonen@aalto.fi).

$E_{cons/mile,n}$	energy consumption for each mile
$prob_l^t(G_y)$	load demand probability being in state y
$prob_R^t(G_x)$	solar irradiance probability being in state x
ψ	complete CPVL model
μ	membership
m	number of objective functions
N_{nd}	number of nondominant solutions
ϕ_b	set of all system nodes
Ω_i	vector that includes all nodes connected to node i

I. Introduction

Worldwide, passive distribution systems are converting to active distribution systems due to the massive utilization of renewable energy sources (RES). Besides the environmental benefits of RES for carbon-neutral societies, these RES can have significant technical benefits to distribution systems, most importantly, loss reductions, voltage improvement, reliability enhancement, and power quality upgrading. Photovoltaic (PV) can be considered the most promising type of RES where it has a flexible and modular structure in which it can be integrated to the grid by utilities, investors, and even final consumers [1]–[3]. A unique feature of this RES type is the watt-var control functions of its inverter, thereby providing local control options [4], [5]. However, this further option is accomplished on the expensive of excessive curtailed power in high penetrated PV distribution systems. Besides, major technical, economic, and controlling penalties can restraint future worldwide strategies to maximize PV hosting capacities in distribution systems.

In parallel with the growing trend of PV, the penetrations of energy storage devices, especially electric vehicles (EVs), have been globally expanding lately. For example, in 2015, the number of different EV variants was reported by the international energy agency, which is a million vehicles [6]. A promising future plan (by 2020) is adopted by the electric vehicle initiative group to utilize 20 million EVs [7]. From the perspective of distribution utilities, EVs can extensively be employed to mitigate the operational problems with high PV penetrations via their controllable built-in batteries. During the parking time of each EV, which is usually the majority of typical days [8], its battery can be considered a valuable control device while considering its charging target. However, the uncontrolled EV demand with its stochastic characteristics can cause potential problems (e.g. line congestion, reverse power flow, and voltage deviation (VD)).

Diverse approaches have been proposed in the literature to optimally size PV in electric distribution systems. In [9], a probabilistic based method has been introduced to determine the optimal size of PV in distribution systems so as to minimize energy losses. Analytical-based methods have been proposed in [10], [11] to place RESs in distribution systems while ignoring their variable generation profiles. The authors of [12] have proposed an analytical-based method that considers load and PV variations to, optimally, integrate one PV unit into distribution systems. In [13], a multi-objective approach has been introduced for the optimal sizing of RES to minimize carbon emissions as well as total costs. In [14], a fast yet accurate energy-loss-assessment approach in distribution systems has been proposed using machine learning, and it has been applied to optimize the PV size. Various optimizers have been employed for solving the RES planning model, e.g. gravitational search optimizer [15], simulated annealing optimizer [16], interior-point optimizer [17], and ant colony optimizer [18]. In [19], different options are considered to incorporate uncertain RES through advanced charging strategies of diverse EV fleets. The authors of [8] have studied the use of electrical storage systems to increase the hosting capacity of RES while alleviating their serious impacts.

As stated above, considerable studies have focused on the optimal sizing of PV in power distribution systems. Nevertheless, several existing methods adopt assumptions due to problem complexity, including single PV sizing, deterministic approaches, ignoring smart functions of the PV inverter, ignoring the option of oversizing the interfacing inverter for allowing extra reactive power support, and/or high active power curtailment. Most importantly, many methods ignore the existence of EVs and so missing the effects of such a vital distribution system component in the integration problem of PV. To effectively decide the size of multiple PVs, diverse charging/discharging control schemes of EV batteries and the smart functions of PV inverters are required to be considered. Driven by the rising trend of EV and the revised IEEE standard, which requires reactive power support from distributed RES units, this work has been directed to the optimal PV sizing direction. Practically, the locations of large PV units are determined by the place which can be bought by the investor. Hence, it is essential to note that we consider predetermined multiple PV sites (by the utility or system planners) as it represents the practical condition while focusing on the stated realistic aspects.

To cover the gap in the literature, a probabilistic sizing approach of multiple PVs in distribution systems with EVs is introduced. The proposed approach minimizes energy losses and VD, and considers different constraints of EV, PV, and distribution systems. The proposed approach considers various EV aspects, including arrival/parting times, the required SOC based on initial SOCs and remaining parking periods, and controlled/uncontrolled charging of batteries. Control schemes of the interfacing PV inverter are also formulated and so optimized by the proposed planning model. In addition, the option for optimally oversizing the PV inverter to allow further reactive power support is also introduced here, and its benefits are highlighted. A two-level multi-objective evolutionary algorithm based on decomposition (MOEA/D) with fuzzy sets is developed to solve this comprehensive bi-level optimization model accurately. The upper level of the developed optimizer accurately optimizes the sizes of multiple PVs, and the lower one optimizes the charging/discharging of EV batteries, inverter oversizing, and reactive power of the PV inverters. The major contributions of the paper can be itemized as follows:

- An optimal sizing approach of multiple PVs in the existence of EVs is proposed.
- The proposed approach prevents active PV power curtailment considering diverse control schemes of the interfacing PV inverter.

- The proposed approach considers PV, EV, and load uncertainties via incorporating their probabilistic models.
- A two-level multi-objective evolutionary algorithm based on decomposition with fuzzy sets is developed to minimize both the total VD and overall energy losses.

II. Optimization Model for PV Sizing

Here, we provide the optimization model for PV sizing in distribution systems interconnected with EVs. Since the energy losses and voltage profiles can be considered the two major issues in distribution systems, they are incorporated as sub-objectives to be minimized in the planning PV model. Regarding the PV energy curtailment, we have considered it as a constraint, where we aimed to prevent the active PV power curtailment. By this way, we can claim that the PV energy curtailment is treated as a sub-objective to be minimized, besides the two sub-objectives. The objective function and the set of constraints for the optimization problem can be expressed as follows.

A. Objective function Formulation

$$\min\{f_1, f_2\} \tag{1}$$

$$\begin{cases} f_1 = \sum_{t=1}^{n_t}\sum_{s=1}^{n_s} E_{l,s}^t \times P_{comb}^t(\lambda_s) & (2) \\ f_2 = \sum_{t=1}^{n_t}\sum_{s=1}^{n_s}\sum_{i=2}^{n_b}\left(\frac{V_{i,s}^t - V_n}{V_n}\right)^2 \times P_{comb}^t(\lambda_s) & (3) \\ E_{l,s}^t = P_{l,s}^t \times \Delta\tau, \quad \forall s,\tau & (4) \end{cases}$$

The set of equations (1)-(4) represent the objective function. The optimization problem defined by (1)-(4) minimizes the expectations of energy losses and VD, in which the probabilities of PV and load are incorporated. The uncertainties of PV and load are represented by a combined PV-load probability (CPVL) model developed using historical datasets where it is described in the next sections. f_1 and f_2 denote the sub-objectives which quantify the total energy losses and VD, respectively. $V_{i,s}$ and V_n are the voltage at bus i and the nominal voltage (1 pu), respectively. $E_{l,s}^t$ and $P_{l,s}^t$ denote the energy losses and power losses of state s, respectively; $\Delta\tau$ is time duration (one hour). $P_{comb}^t(\lambda_s)$ represents the CPVL probability of a particular state s of time duration t. λ_s represents the grouping of the PV and load at state s. n_t is the number of time durations; n_s is the number of all states; n_b is the numbers of buses. The index i starts from 2 to n_b because the VD (f_2) is not a function of the slack bus voltage (i.e. i=1), which equals 1 pu. The primary goal of the optimization problem is to determine the optimal trade-off between voltage improvement and energy loss reductions, where fuzzy sets incorporated in the developed two-level optimizer are employed in this work for this purpose.

B. Constraints

1) PV constraints

$$s.t. \begin{cases} P_{Curt,i,s} \le P_{Curt,i}^{max}, & \forall i \in \phi_b, s \quad (5) \\ S_{Inv,i}^{min} \le S_{Inv,i} \le S_{Inv,i}^{max}, & \forall i \in \phi_b \quad (6) \\ C_{PV,i}^{min} \le C_{PV,i} \le C_{PV,i}^{max}, & \forall i \in \phi_b \quad (7) \\ Q_{Inv,i,s}^{min,t} \le Q_{Inv,i,s}^{t} \le Q_{Inv,i,s}^{max,t}, & \forall i \in \phi_b, s, t \quad (8) \\ \sum_{i=1}^{N_{PV}} P_{PV,i} \le R_{PV}^{max} & (9) \end{cases}$$

The set of equations (5)-(9) represent the constraints of PV. Constraint (5) plays an essential role in the restriction of the active PV power curtailment ($P_{Curt,i}$) by considering the maximum allowed rate ($P_{Curt,i}^{max}$) for each PV unit. Here, to ensure optimal PV sizing while avoiding active PV power curtailment, $P_{Curt,i}^{max}$ is set to be zero. Constraints (6) gives a further option to optimize the oversize rate of the interfacing PV inverter $(S_{Inv,i})$ within its allowed boundaries $(S_{Inv,i}^{min}, S_{Inv,i}^{max})$ by the utilities when sizing the PV units. The sizes of the PV units and the reactive power values ($P_{PV,i}$, $Q_{PV,i}$) are constrained by the corresponding maximum boundaries and minimum boundaries (see (7) and (8)). These boundaries are affected by the present active PV power curtailments and the spare inverter capacity. The maximum total PV size R_{PV}^{max} is adjusted by (9) in which N_{PV} represents the number of PV units. ϕ_b includes the labels of all system nodes.

2) EV constraints

The EV constraints can be described as follows:

$$s.t. \begin{cases} P_{Station,i}^{min,t} \le P_{Station,i,s}^{t} \le P_{Station,i}^{max,t}, & \forall i \in \phi_b, s, t \quad (10) \\ SOC_{n,s}^{t} \ge 1 - DOD_n^{max}, & \forall s, n, t \quad (11) \\ SOC_{n,s}^{Dep} \ge SOC_n^{min}, & \forall n, s \quad (12) \end{cases}$$

Regarding these constraints, for each charging station, the upper and lower limits of active power exchange are symbolized by $P_{Station,i}^{min,t}$ and $P_{Station,i}^{max,t}$, respectively. The active power exchange ($P_{Station,i,s}^{t}$) of EVs is enforced within the upper and lower limits as given by (10). In (11), the current SOC of each individual EV battery is constrained by the adjusted depth of discharge (DOD), thereby following the recommendation of EV manufacturers to regulate DOD for minimizing their degradation rates. In (12), $SOC_{n,s}^{Dep}$ exemplifies the state of charge (SOC) value for n^{th} battery at the parting instantaneous where SOC_n^{min} is the predefined setting to customize the required SOC by the vehicle holder. It is worth mentioning that the optimal charging/discharging powers of EVs depend on the PV and load values at each state. Since there are different states for PV and load at each time duration, there are multiple SOC values for n^{th} battery at the corresponding time duration. Each SOC value has a probability based on CPVL.

3) Distribution system constraints

$$s.t.\quad \begin{cases} \lambda(s,1)P^t_{PV,i} - \lambda(s,2)P^t_{Load,i} \pm P^t_{Station,i,s} - \sum_{j\in\Omega_i} P^t_{ij,s} = 0, \ \forall i \notin \phi_b, s, t & (13) \\ \lambda(s,1)Q^t_{Inv,i,s} - \lambda(s,2)Q^t_{Load,i,s} - \sum_{j\in\Omega_i} Q^t_{ij,s} = 0, \quad \forall i \notin \phi_b, s, t & (14) \\ V^t_{o,s} = 1.0,\ \delta^t_{o,s} = 0.0, \quad \forall s, t & (15) \\ P^t_{o,s} \le P^{t,max}_o,\ Q^t_{o,s} \le Q^{t,max}_o \quad \forall s, t & (16) \\ V^{min} \le V^t_{i,s} \le V^{max}, \quad \forall i \in \phi_b, s, t & (17) \\ I^t_{ij,s} \le I^{\max}_{ij}, \quad \forall ij, s, t & (18) \end{cases}$$

The constraints (13) and (14) represent the active and reactive power mismatches (i.e. equality constraints) in which $P^t_{ij,s}$ and $Q^t_{ij,s}$ power flows through branch ij, respectively. Ω_i is a vector that includes all nodes connected to node i. $P^t_{PV,i}$ and $P^t_{d,s}$ represent the values of the active power of PV and load, respectively. The reactive power of the load is represented by $Q^t_{Load,i}$. V^{min} represents the lower voltage boundary, while V^{max} represents the upper one (17). The main distribution substation is characterized by (15) and (16), whereas its voltage magnitude and angle are symbolized by $V^t_{0,s}$ and $\delta^t_{0,s}$, respectively. The active and reactive power of the main grid $\left(P^t_{o,s}, Q^t_{o,s}\right)$ are constrained within their maximum allowed exchange power rates ($P^{t,max}_{o,s}, Q^{t,max}_{o,s}$). The line flow $I^t_{ij,s}$ is limited by the maximum permitted rates (18). The EV battery and CPVL models are described in the next section.

III. EV BATTERY AND CPVL MODELS

A. Modeling of EV batteries

Here, we describe the charging model of EV batteries complying with the PV sizing in distribution systems. To achieve the charging goal of each individual EV (minimum SOC) according to the charging scheme, the following formula is developed:

$$SOC^t_{n,s} = SOC^{t-1}_{n,s} + \eta_{ch,n} P^t_{ch,n,s} \Delta t \delta - \Delta t \gamma P^t_{dc,n,s} \big/ \eta_{dc,n} \quad (19)$$

in which $P^t_{ch,n,s}$and $P^t_{dc,n,s}$, respectively, symbolize the charging and discharging power rates of n^{th} battery. δ and $\gamma \in \{0,1\}$, where $\delta.\gamma = 0$, for the reason that the battery can work on one mode of operation (i.e., charging mode or discharging mode) at a certain duration. $\eta_{ch,n}$, and $\eta_{dc,n}$ symbolize the efficiencies of the charging and discharging modes, respectively.

The total charging power of an EV station is represented by the sum of the individual power of each battery. For each EV battery, its charging rate is related by its rated capacity ($C_{batt,n}$), its SOC ($SOC^t_{n,s}$), its arrival instant (T_{arr}), and its parting instant ($T_{d,n}$). The charging or discharging power rates of n^{th} EV battery are computed by:

$$P^t_{ch,n,s} = \frac{\left(C_{batt,n} - SOC^t_{n,s} \times C_{batt,n}\right) \times P^t_{Station,i,s}}{T_{rem,n} \times \sum_{j=1}^{m} \frac{1}{T_{rem,j}} \left(C_{batt,j} - SOC^t_{j,s} \times C_{batt,j}\right)} \quad (20)$$

$$P^t_{dc,n,s} = \frac{T_{rem,n} \left(SOC^t_{n,s} \times C_{batt,n}\right) \times P^t_{Station,i,s}}{\sum_{j=1}^{m} T_{rem,j} \left(SOC^t_{j,s} \times C_{batt,j}\right)} \quad (21)$$

where $T_{rem,n}$ is equal to $T_{d,n} - T_{arr,n}$. For each EV station, the aggregator optimally distributes the total charging or discharging powers among the connected vehicles by using the two last formulae ((20) and (21)). In this work, the maximum charging and discharging powers of the EVs are used to be $0.2C_{batt,n}$ [28]. The benefits of these formulae are to ensure fulfilling the charging goal of each EV battery as the charging rate is optimally computed based on its current SOC condition and its remaining parking period. For example, the EV battery with the lowest SOC value or shortest remaining parking period will have the highest partition of the total station power. Based on these features, the proposed model optimizes the charging and discharging rates of all EVs while considering their charging plan in a simultaneous computational process.

Since the variables of EVs have stochastic nature, a probabilistic modeling approach is required. The EV variables include: 1) the arriving instant to the household, 2) parting time, 3) particular daily mileage, and 4) driving practices. The various variants of EVs with different battery types and characteristics are randomly distributed along the day. For each EV, its arrival instant is represented as a random variable with a normal probability density function (pdf) [20]. Then, the EV daily arrival instant is calculated by:

$$f^t_n(T_{arr}) = \exp\left[-(T_{arr} - \mu^t_{T_{arr}})^2 \big/ 2(\sigma^t_{T_{arr}})^2\right] \Big/ (\sigma^t_{T_{arr}} \sqrt{2\pi}) \quad (22)$$

in which $\mu^t_{T_{arr}}$and $\sigma^t_{T_{arr}}$ represent the mean and standard deviation of daily arrival instant, respectively. The corresponding figures of these two parameters, respectively, are 18 and 5 hours [20].

The initial SOC value of an EV battery is related to daily mileage (dm_n), all-electric range (AER_n), and the battery SOC at the preceding parting time. Here, the battery SOC at the preceding parting time is considered to be 100%. In order to extend the lifetime of EV batteries, i.e. minimize their degradation rates, the DOD is incorporated in our model and can be adjusted to have a higher value. It is a fact that higher DOD values can degrade the performance of batteries, and so in our simulations, DOD is set to be 80% [21]. The initial SOC value of each battery is formulated as follows.

$$SOC_{initial,n}(\%) = \begin{cases} (1 - dm_n / AER_n) \times 100, \ 0 < dm_n < 0.8AER_n \\ 20\%, \ dm_n > 0.8AER_n \end{cases} \quad (23)$$

$$AER = C_{batt,n} \big/ E_{cons/mile,n} \quad (24)$$

in which $C_{batt,n,}$ and $E_{cons/mile,n}$ symbolize the nominal rate of the EV battery capacity and energy consumption for each mile, respectively. A lognormal pdf is utilized to model the EV daily mileage [20]:

$$f^t_n(dm) = \frac{1}{dm_n \sqrt{2\pi(\sigma^t_{dm,n})^2}} \times \exp\left[\frac{-(\ln dm_n - \mu^t_{dm,n})^2}{2(\sigma^t_{dm,n})^2}\right], \ dm_n > 0 \quad (25)$$

in which μ^t_{dm}symbolizes the mean of daily mileage while σ^t_{dm}symbolizes the standard deviation of daily mileage. The

corresponding figures of these two later parameters are, respectively, 22.3 and 12.3 miles [20].

B. CPVL Model

The CPVL model involves a unified set of the load demand probability $\left(prob_l^t(G_y)\right)$ and solar irradiance probability $\left(prob_R^t(G_x)\right)$, which is represented by:

$$P_{comb}^t(\lambda_s) = prob_R^t(G_x) \times prob_l^t(G_y) \quad (26)$$

Then, the CPVL model is established by considering all possible PV and load combinations. So, the complete CPVL model ψ is represented by:

$$\psi = \left[\left\{\lambda_s, P_{comb}(\lambda_s)\right\} : s = 1 : n_S\right] \quad (27)$$

in which $P_{com}(\lambda_s)$ includes the elements of the CPVL model based on the matrix λ. It is reported that the Beta pdf is suitable for modeling solar irradiance, and normal pdf is suitable for modeling the load. Note that load demand and solar irradiance are represented as discrete datasets where they are discretized for each time instant into ten regions from 0 to 1.0 (normalized values). The detailed formulation of probabilistic PV and load models can be founded in [9], [17]. The utilization of the CPVL model with the EV models provides comprehensive modeling for the optimal sizing problem of PV in distribution systems.

IV. MOEA/D with Fuzzy Sets

MOEA/D is a recent method of multi-objective evolutionary optimization based on decomposition [22]. This method decomposes the multi-objective optimization problem into several optimization sub-problems. These sub-problems are optimized in a simultaneous manner. Each optimization subproblem can be solved by utilizing the information from its neighboring subproblems only. This method has been demonstrated in many benchmark problems with lower computational complexity and higher-quality solutions [23].

For a multi-objective optimization problem (MOP) with m objective functions, this problem can be decomposed into N scalar optimization sub-problems using Tchebycheff by changing the weight vector $\gamma = (\gamma_1, \gamma_2, \ldots, \gamma_m)^T$, in which $\gamma_i \geq 0$, and $\sum_{i=1}^{m} \gamma_i = 1$. The objective function of a subproblem j is:

$$Minimize\ g^{te}(x|\gamma^j, z^*) = max_{1\leq i\leq m}\{\gamma_i^j | f_i(x) - z^*\} \quad (28)$$

where $\gamma^j = (\gamma_1^j, \ldots, \gamma_m^j)^T$. MOEA/D can minimize all objective functions of the whole sub-problems simultaneously in a single run. g^{te} is the continuation of γ. The solution of the objective function $g^{te}(x|\gamma^i, z^*)$ has to be close to the solution of $g^{te}(x|\gamma^j, z^*)$ if γ^i is close to γ^j. Hence, any information of the sub-problem objective functions that have weight vectors close to γ^i will be very helpful for solving $g^{te}(x|\gamma^i, z^*)$. The algorithm can be described as follows:

Inputs:

- Multi-objective optimization problem.
- A convergence criterion.
- The number of considered subproblems in MOEA/D (N).
- A uniform propagation of N weight vectors: $\gamma^1, \ldots, \gamma^N$.
- The number of weight vectors in the neighborhood of each weight vector (T).

Outputs:

- External Population (EP).

Step 1. Initialization

- Step 1.1. Put EP=0.
- Step 1.2. The Euclidean distances between the weight vectors should be determined, and then the number of the closest weight vectors to each weight vector should be found out. For each $i=1,\ldots, N$, put $B(i)= \{i_1,\ldots,i_N\}$, where $\gamma^{i1},\ldots, \gamma^{iN}$ are the numbers of the closest weight vectors to the vector γ^i (T); $B(i)$ contains the indexes of these vectors.
- Step 1.3. Generation of an initial population $x^1,\ldots,x^N$ arbitrary. Put $FV^i=F(x^i)$, where FV^i if the F-value of x^i.
- Step 1.4. $z=(z_1,\ldots,z_m)^T$ should be initialized using the problem-specific method, where z_i is the best value found so far for objective f_i.

Step 2. Update

For $i=1,\ldots, N$, do

- Step 2.1. Reproduction: From $B(i)$, select two indexes k and l arbitrary, and from x^k and x^l, compute a new solution y by utilizing genetic operators.
- Step 2.2. Improvement: Produce y' by applying a problem specific repair/improvement heuristic on y.
- Step 2.3. Update of z: For $j=1,\ldots, m$, if $z_j < f_j(y')$, then $z_j=f_j(y')$.
- Step 2.4. Update the neighbor solution: For each $j \in B(i)$, if $g^{te}(y'|\gamma^j,z) \leq g^{te}(x^j|\gamma^j,z)$, then $x^j=y'$ and $FV^j=F(y')$.
- Step 2.5. Update the External Population:
  - Remove all vectors dominated by $F(y')$ from EP.
  - Add $F(y')$ to EP if there are no vectors in EP dominate it.

Step 3. Termination:

If the convergence criterion is met, stop and print the outputs (i.e., EP). Otherwise, go to *Step 2*. The maximum number of iterations or firmness of EP in successive iterations can be used as a stopping criterion.

After obtaining the Pareto solutions, it is essential to choose the best-compromised solution amongst these solutions. Therefore, the fuzzy logic theory is employed for this purpose [24]. The best solution is the solution that has the smallest distance from the ideal solution and the furthest distance from the worst one. For a minimization problem, the best and the worst values of the objective function can be denoted by, respectively, OF_i^{min} and OF_i^{max}. The lowest and highest satisfaction can be decided based on the value of the membership (μ) in which 0 means the lowest satisfaction, and 1 implies the highest satisfaction. The membership value of k^{th} nondominant solution for i^{th} objective function can be formulated as follows:

$$\mu_i^k = \left(OF_i^{max} - OF_i\right) \Big/ \left(OF_i^{max} - OF_i^{min}\right) \quad (29)$$

For each k, the membership function can be normalized as follows:

$$\mu^k = \sum_{i=1}^{m} \mu_i^k \Big/ \sum_{k=1}^{N_{nd}} \sum_{i=1}^{m} \mu_i^k \quad (30)$$

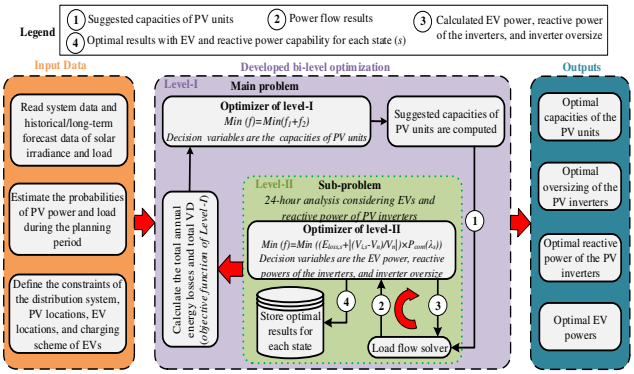

Fig.1. Solution process of the proposed approach.

where m and N_{nd} are the number of objective functions and number of non-dominant solutions, respectively.

V. Solution Process

The solution procedure of the proposed approach for computing the optimal capacities of PV units and their inverter oversize considering EVs and reactive power capability of the PV inverters is illustrated in Fig. 1. It can be seen from this figure that the solution procedure consists of three main stages: 1) input data, 2) developed bi-level optimization, and 3) outputs. In the input data stage, the distribution system data and historical/long-term forecast data of solar irradiance and load are read. Moreover, the probabilities of PV power and load are determined in this stage; hence the combined probability can be computed. Furthermore, constraints of the PV, EVs, and distribution systems are specified. Also, PV locations, EV locations, and charging schemes of EV are read. In the second stage, a bi-level optimization model is developed to calculate the optimal capacities of the PV units and the optimal oversize of their interfacing inverters in the presence of EVs and the reactive power capability of the inverters. The proposed model can be solved in one level, but we select to divide the optimization model in two levels. This two-levels approach greatly minimizes the size of the overall optimization problem with a high accuracy rate. This two-levels approach is widely used in large-scale optimization, which is called master-slave optimization, as it scales well with the size of the problem. MOEA/D is used in the developed bi-level optimization model. The main problem is solved in level-I while the sub-problem is solved in level-II.

Suggested capacities of PV units are computed in the level-I by the optimizer of this level while the charging/discharging power of EVs and reactive power of the PV inverters have to be considered in the planning model. Therefore, the optimal charging/discharging power of EVs, inverter oversizing, and reactive power of the PV inverters are determined in the level-II, which is a sub-problem of the whole planning problem. Note that the PV power is computed considering the maximum power point tracking (MPPT) of the interfacing inverter described in [9].

Hence, for each state, the optimizer of level-II suggests the charging/discharging power of EVs, inverter oversize, and reactive power of the PV inverters. These control variables and the capacities of the PV units, which are calculated in level-I, are sent to a power flow solver proposed in [25] to calculate the objective functions for that state (energy losses and VD). The results of the power flow are sent back to the optimizer of level-II to compare the current and previous values of the objective functions. This process is repeated for the corresponding state until the optimizer converges to determine the optimal power of EVs, inverter oversize, and reactive power of the PV inverters. Then the optimal results of the whole states are stored. The summations of the objective functions are used as objective functions of the level-I.

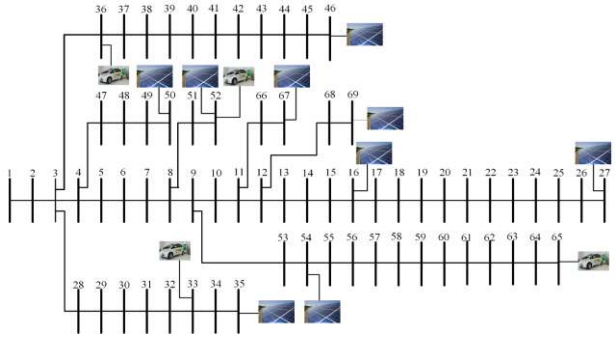

Fig. 2. Single line diagram of the 69-bus distribution system.

As displayed in Fig. 1, the second stage is a bi-level optimization model where level-I comprises level-II. Therefore, level-II must be wholly executed until its convergence for each iteration of level-I. This process is repeated until the level-I is converged. The optimal outputs are given in the third stage, including optimal capacities of PV units, optimal inverter oversize, optimal reactive power of the inverters, and optimal charging/discharging power of EVs.

VI. Results and Discussion

The IEEE 69-Bus distribution system shown in Fig. 2 is utilized to reveal the efficacy of the proposed approach. The data of this system are taken from [26]. The PV units are assumed to be connected at nine different locations, as shown in Fig. 2. Four EV charging stations are supposed to be connected at four different locations (33, 36, 52, and 65), as depicted in Fig. 2. Each station can accommodate up to 60 EVs. The distribution of the EVs throughout the whole day can be computed based on (22). The initial SOC of each EV can be calculated by (23).

The EVs with Tesla Model S batteries are used in this work. Each battery of this model has a capacity of 85 kWh [27]. Each EV is assumed to be parked and connected to the distribution system for 12 hours. To satisfy the requirements of the EV's owners at the departure time, the minimum SOC which is predefined by the owners should be considered in the optimization model. The maximum charging and discharging powers of the EVs are used to be $0.2C_{batt,n}$ [28]. According to the standard given in [29], the lower and upper voltage limits are 0.95 p.u. and 1.05 p.u., respectively. The maximum curtailment power of PV is zero for preventing the curtailing of the output PV power. The minimum SOC of the EVs at departing time is assumed to be 80%. The upper and lower limits of the active power exchange of EVs depend on the number of the existing EVs and their SOC values. The minimum and maximum reactive powers of the interfacing

TABLE I
RESULTS OF THE DIFFERENT SCENARIOS

Item	Bus	Scenario 0	Scenario 1	Scenario 2	Scenario 3
PV capacity (kW)	16	-	213	380	271
	27	-	380	320	367
	35	-	156	226	128
	46	-	337	140	198
	50	-	260	189	7
	52	-	299	380	210
	55	-	339	380	140
	67	-	349	350	371
	69	-	75	234	324
Total PV capacity (kW)		0	2408	2599	2016
Energy loss (MWh)		1771	1473	1445	1398
Average VD (pu)		0.19	0.12	0.11	0.11
Average SOC (%)		100	100	100	93

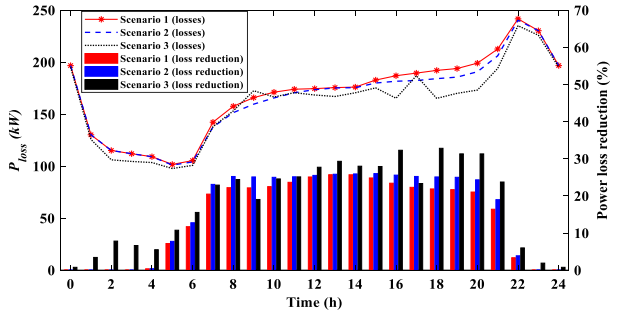

Fig. 3. Active power loss and loss reduction in the distribution system.

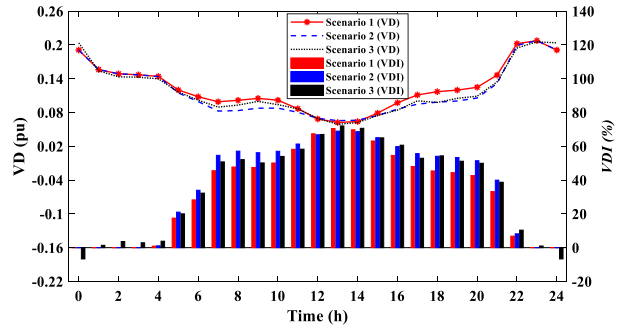

Fig. 4. Voltage deviation and voltage deviation improvement in the distribution system.

inverter depend on the spare capacity of the inverter considering the adopted inverter oversize. The maximum limit of the PV inverter oversizing is 100% of the inverter rating. The maximum size of each PV unit is 400 kW while the maximum penetration of the total PV units with respect to the load is 100%. The proposed approach is executed with and without considering the reactive power capability of the interfacing inverters of PV units. The historical data of solar irradiance and load for three years are utilized to generate their probabilities. The whole years are portrayed by a day throughout these years. We have written the code of the optimization problem (MOEA/D optimization algorithm and the planning model of PV) in MATLAB 2017b, and this program has been carried out on a Core I5 PC with 8GB RAM.

A. *Optimal Integration of PV units*

Here, the optimal sizes of the PV units to minimize the annual energy losses and VD at PCC (at PV and EVs buses) are determined. Three different scenarios are performed and compared to the base scenarios without considering the

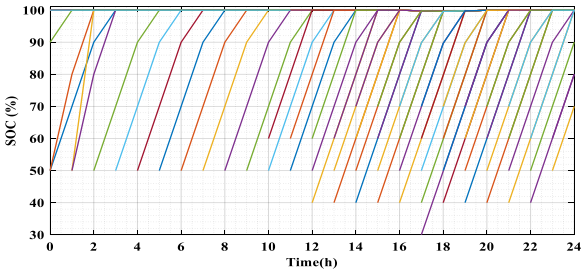

Fig. 5. SOC of 60 EVs using uncontrolled charging technique for Scenario 0, Scenario 1, and Scenario 2 (Each line represents the SOC behavior of an EV battery).

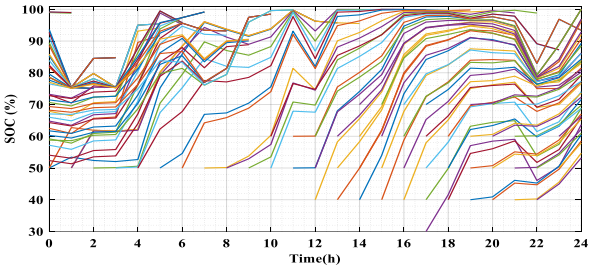

Fig. 6. SOC of 60 EVs connected to charging station at bus 33 using optimal charging/discharging technique for Scenario 3.

reactive power capability of the PV inverters. These scenarios can be described as follows:

Scenario 0: the base scenario where there are no PVs interconnected to the grid while EVs charge with the uncontrolled technique.

Scenario 1: in this scenario, the optimum PV capacities are determined without considering the uncontrolled EV charging.

Scenario 2: in this scenario, the optimal capacities of PVs are determined considering the uncontrolled EV charging.

Scenario 3: here, the optimal capacities of PV units are determined considering the optimal EV charging/discharging.

Note that in the case of uncontrolled EV charging, the EVs start to charge once they are plugged to the charging station with a fixed rate ($0.2\ C_{batt}$). The results of the base scenario and the different three scenarios are given in Table I and Figs. 3 and 4. From these results, it is observed that the annual energy losses and the VD are significantly reduced by applying the three different scenarios (Scenario 1- Scenario 3) compared to the base scenario (Scenario 0), especially during the day time in which there are active power generations from the PV units. Furthermore, we can observe that considering EVs in the optimization problem (Scenarios 2 and 3) can do a great job in minimizing the annual energy losses and improving the VD compared to Scenario 1. Also, the charging/discharging technique of the EVs has a pronounced impact on the annual energy losses and VD in which considering the optimal charging/discharging technique (Scenario 3) provides higher energy loss reduction compared to the other scenarios.

The annual energy losses are 1771 MWh, 1473 MWh, 1445 MWh, and 1398 MWh while the average VDs are 0.19 pu, 0.12 pu, 0.11 pu, and 0.11 pu for Scenario 0, Scenario 1, Scenario 2, and Scenario 3, respectively. On the other hand, the optimal capacities of the PV units depend on the applied scenario, which are determined by the proposed optimizer. For

TABLE II
RESULTS OF SCENARIOS 4, 5, AND 6

Item	Bus	Scenario 4	Scenario 5	Scenario 6
PV capacity (kW)	16	171	353	331
	27	242	380	296
	35	293	250	291
	46	331	95	44
	50	271	248	366
	52	349	133	343
	55	346	348	345
	67	244	241	214
	69	254	174	303
Total PV capacity (kW)		2501	2222	2533
Energy loss (MWh)		1354	1303	1251
Average VD (pu)		0.10	0.09	0.08
Average SOC (%)		100	96	94

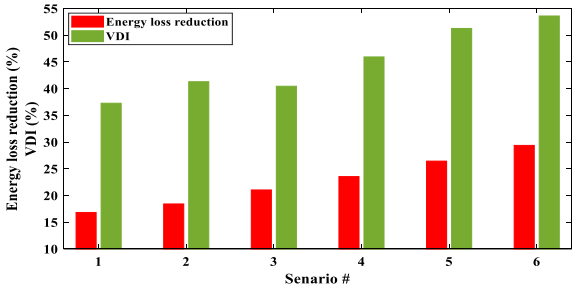

Fig. 7. Annual energy loss reduction and voltage deviation improvement for Scenarios 1-6 with respect to Scenario 0.

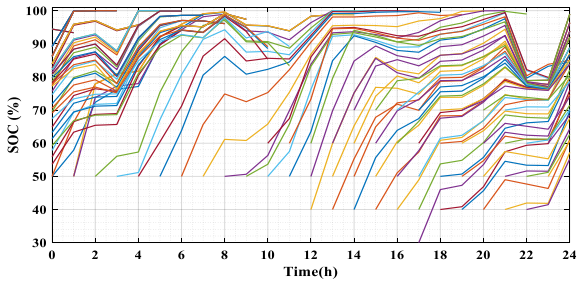

Fig. 8. SOC of 60 EVs connected to charging station at bus 33 using optimal charging/discharging technique for Scenario 5.

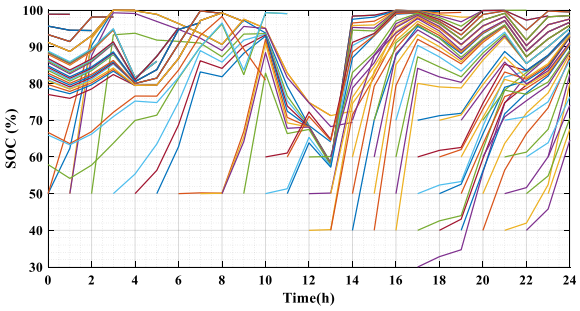

Fig. 9. SOC of 60 EVs connected to charging station at bus 33 using optimal charging/discharging technique for Scenario 6.

instance, the optimal capacities of the PV units at bus 27 are 380 kW, 320 kW, and 367 kW for Scenario 1, Scenario 2, and Scenario 3, respectively. However, the optimal capacities of the PV units at bus 50 are 260 kW, 189 kW, and 7 kW for Scenarios 1, 2, and 3, respectively. Note that we have considered the minimum constraint of the PV source, at each location, to be zero in this work. The total capacity of PV units in the case of Scenario 2 is 2599 kW, which is higher than those of Scenarios 1 and 3 (2408 kW and 2016 kW). It worth mentioning that the average SOC at the departure time is 100% in the case of Scenarios 0-2, while it is 93% in the case of Scenario 3. This indicates that the proposed approach, besides minimizing the annual energy losses and VD, satisfies the EVs owner's requirements.

The SOC profiles of the EVs, which are charged using the uncontrolled charging technique in the case of Scenario 0, Scenario 1, and Scenario 2 (it is the same for the four charging stations) are given in Fig. 5. It can be observed that the EVs are fully charged in a short period while the discharging option is deactivated in those scenarios. The SOC of the EVs using optimal charging/discharging technique (Scenario 3) of the charging station, which are connected to bus 33, is shown in Fig. 6. It is clear from this figure that the SOC of all EVs at the departure time is high (more than 80%) and enough for daily driving. The EVs that arrive at the end of the previous day have been considered in the planning problem where they would continue charging at the beginning of the sample day. It worth mentioning that the SOC of EVs which are connected to charging stations at buses 36, 52, and 65 have different tendencies, but they are high enough and fulfill the owner's requirements at the departure time. The results are expected to be changed if the minimum SOC at departure time is changed from 80% to 100%, where the optimizer can work accordingly. Specifically, the objectives may be slightly higher due to the further limitations of the charging energy of EVs to reach the extended SOC limit. However, in this work, we follow a recommendation that 100% SOC is not preferred because of lifespan considerations [30], [31]. From these results, it can be noted that considering the EVs in the planning problem has a noticeable positive impact on reducing the annual energy losses and VD in the distribution system while satisfying the preferences of EV's owners at the parting time.

B. Optimal Integration of PV units Considering Reactive Power Capability of the Interfacing Inverters

In this subsection, the optimal capacities of PV units are computed, considering the reactive power capability of the interfacing inverters. For this purpose, three scenarios are studied as follows:

Scenario 4: in this scenario, the optimal capacities of the PV units are computed considering the reactive power capability of the PV inverters and uncontrolled charging of EVs.

Scenario 5: in this scenario, the optimal capacities of the PV units are computed considering the reactive power capability of the PV inverters and the optimal charging/discharging of EVs.

Scenario 6: this scenario is like Scenario 5, but the maximum charging and discharging powers of the EVs are used to be $0.5C_{batt,n}$ instead of $0.2C_{batt,n}$ in the case of Scenario 5.

Table II shows the results of these three scenarios. From this table, by employing the reactive power capability of the PV inverters, the annual energy loss and the VD are decreased compared to the previous scenarios (Scenarios 0-3). For instance, the annual energy losses are 1354 MWh, 1303 MWh, and 1251 MWh, while the average VD values are 0.10 pu, 0.09 pu, and 0.08 for Scenarios 4, 5, and 6, respectively. Fig. 7 compares all scenarios in terms of annual energy loss reduction and voltage deviation improvement (VDI) with respect to the base scenario (Scenario 0). It is clear that Scenarios 4, 5, and 6 have higher loss reduction and VDI than the rest scenarios. However, loss reduction and VDI in the

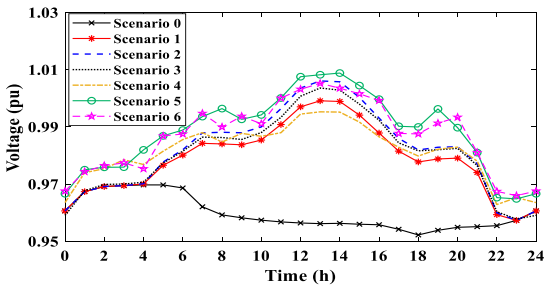

Fig. 10. Voltage profiles at bus 27 for the whole scenarios.

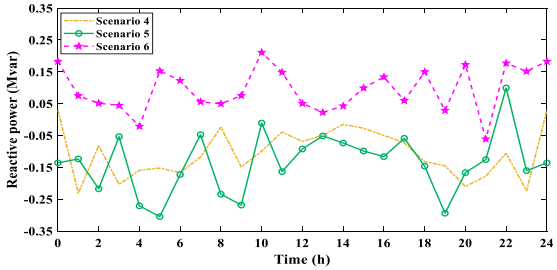

Fig. 11. Injected/absorbed reactive power of the PV inverter for Scenarios 4, 5, and 6.

TABLE III
RESULTS OF SCENARIO 6 CONSIDERING ONLY ANNUAL ENERGY LOSSES

Location	PV capacity (kW)	Energy loss (MWh)	Average VD (pu)	Total PV capacity (kW)
16	215	1109	0.14	2284
27	354			
35	124			
46	346			
50	355			
52	36			
55	182			
67	325			
69	347			

TABLE IV
RESULTS OF SCENARIO 6 CONSIDERING ONLY VD

Location	PV capacity (kW)	Energy loss (MWh)	Average VD (pu)	Total PV capacity (kW)
16	378	1342	0.07	2657
27	377			
35	230			
46	206			
50	347			
52	152			
55	353			
67	304			
69	310			

case of Scenario 6 is better than those in the case of Scenarios 4 and 5.

Furthermore, employing the reactive power capability of the PV inverters and changing the maximum charging and discharging powers of the EVs have an effect on the optimal capacities of the PV units, as illustrated in Table II. For instance, the optimal capacities of the PV units at bus 50 are 271 kW, 248 kW, and 366 kW for Scenarios 4, 5, and 6, respectively. The total capacity of PV units in the case of Scenario 6 is 2533 kW, which is higher than those of Scenarios 4 and 5 (2501 kW and 2222 kW). Also, the average SOC of the EVs is high enough for daily driving. By comparing Scenarios 5 and 6 in Table II with Scenario 3 in Table I (where the optimal charging/discharging technique of EVs is used in these scenarios), the average SOC values in Scenarios 5 and 6 (96% and 94%) are higher than that in Scenario 3 (93%). Therefore, employing the reactive power capability of the PV inverters and increasing the maximum limit of charging and discharging powers of the EVs have a positive impact on SOC of the EVs. The SOC of the EVs connected to the charging station at bus 33 for Scenarios 5 and 6 are presented in Figs. 8 and 9, respectively. On the other hand, the SOC of the EVs in the case of Scenario 4 is the same as Fig. 5.

To compare the voltages at PCC and the reactive power of the PV inverters in the case of all scenarios, bus 27 is used for this purpose in which it is the farthest from the slack bus (assumed to be bus 1) and has a PV unit. The other buses with PV units follow the same trend as that bus. Therefore, to avoid the repetition of the results, only the results at bus 27 are demonstrated. The voltage profiles at that bus (bus 27) for different scenarios are shown in Fig. 10. We can observe that the voltage profile is improved by applying the Scenarios 1-6 compared to the base scenario (Scenario 0). However, at the night period, Scenarios 1-3 cannot improve the voltage profile in which the active power generations of the PV units are zero, and the reactive power capability of the PV inverters is deactivated in these scenarios. In contrast, the voltage profile is improved during the night-time in the case of Scenarios 4, 5, and 6, thanks to the activation of the reactive power capability of the PV inverters. The injected/absorbed reactive power of the PV inverter in these scenarios is given in Fig. 11 in which the negative means injected reactive power from the inverter while the positive means absorbed reactive power.

C. Performance evaluation of the proposed approach

Here, we demonstrate the effectiveness of the proposed approach to determine the trade-off between voltage improvement and energy loss reductions (i.e. best-compromised solution). For this purpose, we have studied the performance of the proposed approach (with Scenario 6) by considering two cases (Cases 1 and 2). In Case 1, the proposed approach considers only the annual energy losses to be minimized. In turn, the proposed approach considers only the VD in Case 2. Tables III and IV show the results of Cases 1 and 2, respectively. As noticed, the annual energy losses and the average VD of Case 1 are 1109 MWh and 0.14 pu, while they are 1342 MWh and 0.07 pu with Case 2. By comparing these results with the results of the proposed multi-objective approach with Scenarios 6 in table II, the proposed approach can determine the best-compromised solution considering the trade-off between the two sub-objectives. For instance, the proposed approach in Table II achieves VD value of 0.08 pu, which is low compared with Case 1 with a slight increase in the annual energy losses (1251 MWh). Further, the proposed approach in Table II achieves lower annual energy losses compared with Case 2 with a higher VD value. This analysis demonstrates the benefits of the proposed approach, which considers the trading between two sub-objectives in the planning model of PV.

D. Inverter Oversizing Impact on the Optimal PV Sizing

Here, the impact of the oversizing of the PV inverters is studied in which the interfacing inverter is often fully loaded during high PV power generation. Therefore, by oversizing

TABLE V
RESULTS OF SCENARIO 5 CONSIDERING INVERTER OVERSIZING

Location	PV capacity (kW)	Oversizing (%)	Energy loss (MWh)	Average VD (pu)	Total PV capacity (kW)
16	319	89	1262	0.08	2600
27	240	60			
35	360	46			
46	190	50			
50	243	99			
52	380	89			
55	372	86			
67	280	88			
69	216	94			

the inverters, further reactive power will be available to be injected/absorbed from/by the inverters. In this analysis, the inverter oversizing is optimally computed to reduce the annual energy losses and improve the VD considering the maximum limit of the oversizing not to be more than 100% of the inverter rating. Scenario 5 has been applied here, and its results are demonstrated in Table V. Form this table we can see that by oversizing the interfacing inverters, the annual energy losses and VD are significantly decreased compared to the same scenario in Table II and the rest scenarios in Table I and Table II (1 to 4). Furthermore, by optimally oversizing the PV inverters, the total capacity of PV units in the distribution system is increased by 17%, in which the total capacity of PV units is increased from 2222 kW for Scenario 5 in Table II (without inverter oversizing) to 2600 kW for Scenario 5 in Table V.

VII. CONCLUSIONS

Severe operational issues can be observed in the distribution systems due to PV generation variability and EV stochastic characteristics. In this paper, a probabilistic sizing approach of multiple PVs in EV-hosted distribution systems has been proposed. The proposed approach considers various realistic aspects of uncertain PVs and EVs. A two-level MOEA/D with fuzzy sets has been developed to solve the comprehensive bi-level optimization model for optimizing the sizes of PVs while considering various charging schemes of EVs and preventing active PV power curtailment. The effectiveness of the proposed approach has been demonstrated on the 69-bus distribution systems with 4 EV stations and 9 PV sites considering historical datasets. The control schemes of EV charging and the interfacing PV inverters can significantly affect the optimal sizes of multiple PV units. Specifically, controlled EV battery schemes can allow a higher reduction in the objective function compared with uncontrolled ones. Similar benefits can also be achieved by enabling reactive power support from PV inverters. In addition, oversizing the PV inverters can provide further improvement in terms of loss reduction and voltage regulations, besides increasing the PV hosting capacity in distribution systems. In future work, the PV installation costs will be considered in the sizing model of PV.

REFERENCES

[1] B. Mohandes, M. S. El Moursi, N. Hatziargyriou, and S. El Khatib, "A Review of Power System Flexibility With High Penetration of Renewables," *IEEE Trans. Power Syst.*, vol. 34, no. 4, pp. 3140–3155, Jul. 2019, doi: 10.1109/TPWRS.2019.2897727.

[2] H. Sun *et al.*, "Review of Challenges and Research Opportunities for Voltage Control in Smart Grids," *IEEE Trans. Power Syst.*, vol. 34, no. 4, pp. 2790–2801, Jul. 2019, doi: 10.1109/TPWRS.2019.2897948.

[3] D. N. Sidorov *et al.*, "A Dynamic Analysis of Energy Storage with Renewable and Diesel Generation using Volterra Equations," *IEEE Trans. Ind. Informatics*, pp. 1–1, 2019, doi: 10.1109/TII.2019.2932453.

[4] A. Datta, R. Sarker, and I. Hazarika, "An Efficient Technique Using Modified *p–q* Theory for Controlling Power Flow in a Single-Stage Single-Phase Grid-Connected PV System," *IEEE Trans. Ind. Informatics*, vol. 15, no. 8, pp. 4635–4645, Aug. 2019, doi: 10.1109/TII.2018.2890197.

[5] H. Rezk, M. Aly, M. Al-Dhaifallah, and M. Shoyama, "Design and Hardware Implementation of New Adaptive Fuzzy Logic-Based MPPT Control Method for Photovoltaic Applications," *IEEE Access*, vol. 7, pp. 106427–106438, 2019, doi: 10.1109/ACCESS.2019.2932694.

[6] E. V Global, "Outlook 2016: Beyond One Million Electric Cars," *Int. Energy Agency Paris, Fr.*, 2016.

[7] E. A. M. Association and others, "A Review of Battery Technologies for Automotive Applications," Brussels, Belgium, 2014. [Online]. Available: https://www.acea.be/publications/article/a-review-of-battery-technologies-for-automotive-applications.

[8] N. G. Paterakis and M. Gibescu, "A methodology to generate power profiles of electric vehicle parking lots under different operational strategies," *Appl. Energy*, vol. 173, pp. 111–123, Jul. 2016, doi: 10.1016/J.APENERGY.2016.04.024.

[9] Y. M. Atwa, E. F. El-Saadany, M. M. A. Salama, and R. Seethapathy, "Optimal Renewable Resources Mix for Distribution System Energy Loss Minimization," *IEEE Trans. Power Syst.*, vol. 25, no. 1, pp. 360–370, 2010, doi: 10.1109/TPWRS.2009.2030276.

[10] M. Vatani, G. B. Gharehpetian, M. J. Sanjari, and D. Solati Alkaran, "Multiple distributed generation units allocation in distribution network for loss reduction based on a combination of analytical and genetic algorithm methods," *IET Gener. Transm. Distrib.*, vol. 10, no. 1, pp. 66–72, Jan. 2016, doi: 10.1049/iet-gtd.2015.0041.

[11] D. Q. Hung and N. Mithulananthan, "Multiple Distributed Generator Placement in Primary Distribution Networks for Loss Reduction," *IEEE Trans. Ind. Electron.*, vol. 60, no. 4, pp. 1700–1708, Apr. 2013, doi: 10.1109/TIE.2011.2112316.

[12] D. Q. Hung, N. Mithulananthan, and K. Y. Lee, "Determining PV Penetration for Distribution Systems With Time-Varying Load Models," *IEEE Trans. Power Syst.*, vol. 29, no. 6, pp. 3048–3057, Nov. 2014, doi: 10.1109/TPWRS.2014.2314133.

[13] V. Vahidinasab, "Optimal distributed energy resources planning in a competitive electricity market: Multi-objective optimization and probabilistic design," *Renew. Energy*, vol. 66, pp. 354–363, Jun. 2014, doi: 10.1016/J.RENENE.2013.12.042.

[14] K. Mahmoud and M. Abdel-Nasser, "Fast yet Accurate Energy-Loss-Assessment Approach for Analyzing/Sizing PV in Distribution Systems Using Machine Learning," *IEEE Trans. Sustain. Energy*, vol. 10, no. 3, pp. 1025–1033, Jul. 2019, doi: 10.1109/TSTE.2018.2859036.

[15] A. Ali, D. Raisz, K. Mahmoud, and M. Lehtonen, "Optimal Placement and Sizing of Uncertain PVs Considering Stochastic Nature of PEVs," *IEEE Trans. Sustain. Energy*, pp. 1–1, 2019, doi: 10.1109/TSTE.2019.2935349.

[16] J. Mitra, M. R. Vallem, and C. Singh, "Optimal Deployment of Distributed Generation Using a Reliability Criterion," *IEEE Trans. Ind. Appl.*, vol. 52, no. 3, pp. 1989–1997, May 2016, doi: 10.1109/TIA.2016.2517067.

[17] A. Ali, D. Raisz, and K. Mahmoud, "Optimal oversizing of utility-owned renewable DG inverter for voltage rise prevention in MV distribution systems," *Int. J. Electr. Power Energy Syst.*, vol. 105, pp. 500–513, Feb. 2019, doi: 10.1016/J.IJEPES.2018.08.040.

[18] H. Bagheri Tolabi, M. H. Ali, and M. Rizwan, "Simultaneous Reconfiguration, Optimal Placement of DSTATCOM, and Photovoltaic Array in a Distribution System Based on Fuzzy-ACO Approach," *IEEE Trans. Sustain. Energy*, vol. 6, no. 1, pp. 210–218, Jan. 2015, doi: 10.1109/TSTE.2014.2364230.

[19] K. Seddig, P. Jochem, and W. Fichtner, "Integrating renewable energy sources by electric vehicle fleets under uncertainty," *Energy*, vol. 141, pp. 2145–2153, Dec. 2017, doi: 10.1016/J.ENERGY.2017.11.140.

[20] K. Qian, C. Zhou, M. Allan, and Y. Yuan, "Modeling of Load Demand Due to EV Battery Charging in Distribution Systems," *IEEE Trans. Power Syst.*, vol. 26, no. 2, pp. 802–810, May 2011, doi: 10.1109/TPWRS.2010.2057456.

[21] B. Hashemi, M. Shahabi, and P. Teimourzadeh-Baboli, "Stochastic-

Based Optimal Charging Strategy for Plug-In Electric Vehicles Aggregator under Incentive and Regulatory Policies of DSO," *IEEE Trans. Veh. Technol.*, vol. 68, no. 4, pp. 3234–3245, 2019, doi: 10.1109/TVT.2019.2900931.

[22] Q. Zhang and H. Li, "MOEA/D: A multi-objective evolutionary algorithm based on decomposition," *IEEE Trans. Evol. Comput.*, vol. 11, no. 6, pp. 712–731, 2007, doi: 10.1109/TEVC.2007.892759.

[23] Hui Li and Qingfu Zhang, "Multi-objective Optimization Problems With Complicated Pareto Sets, MOEA/D and NSGA-II," *IEEE Trans. Evol. Comput.*, vol. 13, no. 2, pp. 284–302, Apr. 2009, doi: 10.1109/TEVC.2008.925798.

[24] S. Roy Ghatak, S. Sannigrahi, and P. Acharjee, "Multi-Objective Approach for Strategic Incorporation of Solar Energy Source, Battery Storage System, and DSTATCOM in a Smart Grid Environment," *IEEE Syst. J.*, vol. 2, pp. 1–12, 2018, doi: 10.1109/JSYST.2018.2875177.

[25] K. Mahmoud and N. Yorino, "Robust quadratic-based BFS power flow method for multi-phase distribution systems," *IET Gener. Transm. Distrib.*, vol. 10, no. 9, pp. 2240–2250, Jun. 2016, doi: 10.1049/iet-gtd.2015.1518.

[26] M. E. Baran and F. F. Wu, "Network reconfiguration in distribution systems for loss reduction and load balancing," *IEEE Trans. Power Deliv.*, vol. 4, no. 2, pp. 1401–1407, Apr. 1989, doi: 10.1109/61.25627.

[27] X. Wu, X. Hu, S. Moura, X. Yin, and V. Pickert, "Stochastic control of smart home energy management with plug-in electric vehicle battery energy storage and photovoltaic array," *J. Power Sources*, vol. 333, pp. 203–212, 2016, doi: 10.1016/j.jpowsour.2016.09.157.

[28] S. Shafiee, M. Fotuhi-Firuzabad, and M. Rastegar, "Investigating the Impacts of Plug-in Hybrid Electric Vehicles on Power Distribution Systems," *IEEE Trans. Smart Grid*, vol. 4, no. 3, pp. 1351–1360, Sep. 2013, doi: 10.1109/TSG.2013.2251483.

[29] "Australian Standard AS/NZS 61000.3.100:2011, Electromagnetic compatibility (EMC) – Limits – Steady state voltage limits in public electricity systems." 2011.

[30] G. Ning, B. Haran, and B. N. Popov, "Capacity fade study of lithium-ion batteries cycled at high discharge rates," *J. Power Sources*, vol. 117, no. 1–2, pp. 160–169, 2003, doi: 10.1016/S0378-7753(03)00029-6.

[31] E. Wikner and T. Thiringer, "Extending Battery Lifetime by Avoiding High SOC," *Appl. Sci.*, vol. 8, no. 10, p. 1825, 2018, doi: 10.3390/app8101825.

Abdelfatah Ali received the B.Sc. degree and the M.Sc. degree in electrical engineering from Aswan University, Aswan, Egypt, in 2009 and 2013, respectively. In 2020, he received the Ph.D. degree from the Doctoral School of Electrical Engineering, Budapest University of Technology and Economics, Budapest, Hungary. Since 2010, he has been an Assistant Lecturer with the Faculty of Engineering, South Valley University (SVU), Qena, Egypt. He is currently working as an Assistant Professor with SVU. His research interests include modeling, analysis, control, and optimization of power systems with distributed generation and electric vehicles.

Karar Mahmoud received the Ph.D. degree from the Electric Power and Energy System Laboratory (EPESL), Graduate School of Engineering, Hiroshima University, Hiroshima, Japan, in 2016. Since 2010, he has been with Aswan University (Egypt), where he is presently an Assistant Professor at the Electrical Engineering Department. He is currently a Postdoctoral Researcher with the School of Electrical Engineering, Aalto University, Finland. He has authored or coauthored more than 60 publications in top-ranked journals (including +10 IEEE journals), international conferences, and book chapters. His research interests include power systems, renewable energy sources, smart grids, distributed generation, electric vehicles, distributed system management, optimization, and applied machine/deep learning.

Matti Lehtonen received the M.S. and Licentiate degrees in electrical engineering from the Aalto University School of Science and Technology (formerly Helsinki University of Technology), Espoo, Finland, in 1984 and 1989, respectively, and the D.Sc. degree from the Tampere University of Technology, Tampere, Finland, in 1992. Since 1987, he has been with VTT Energy, Espoo, and since 1999, he has been with the School of Electrical Engineering, Aalto University, where he is a Professor of IT applications in power systems. His main activities include earth fault problems, harmonic related issues, and applications of information technology in distribution automation and distribution energy management.